

# High-Performance Organic Electrochemical Transistors Achieved by Optimizing Structural and Energetic Ordering of Diketopyrrolopyrrole-Based Polymers

Il-Young Jo, Dahyun Jeong, Yina Moon, Dongchan Lee, Seungjin Lee, Jun-Gyu Choi, Donghyeon Nam, Ji Hwan Kim, Jinhan Cho, Shinuk Cho, Dong-Yu Kim, Hyungju Ahn, Bumjoon J. Kim,\* and Myung-Han Yoon\*

For optimizing steady-state performance in organic electrochemical transistors (OECTs), both molecular design and structural alignment approaches must work in tandem to minimize energetic and microstructural disorders in polymeric mixed ionic–electronic conductor films. Herein, a series of poly(diketopyrrolopyrrole)s bearing various lengths of aliphatic–glycol hybrid side chains (PDPP-*m*EG; *m* = 2–5) is developed to achieve high-performance p-type OECTs. PDPP-4EG polymer with the optimized length of side chains exhibits excellent crystallinity owing to enhanced lamellar and backbone interactions. Furthermore, the improved structural ordering in PDPP-4EG films significantly decreases trap state density and energetic disorder. Consequently, PDPP-4EG-based OECT devices produce a mobility–volumetric capacitance product ( $[\mu C^*]$ ) of  $702 \text{ F V}^{-1} \text{ cm}^{-1} \text{ s}^{-1}$  and a hole mobility of  $6.49 \pm 0.60 \text{ cm}^2 \text{ V}^{-1} \text{ s}^{-1}$ . Finally, for achieving the optimal structural ordering along the OECT channel direction, a floating film transfer method is employed to reinforce the unidirectional orientation of polymer chains, leading to a substantially increased figure-of-merit  $[\mu C^*]$  to over  $800 \text{ F V}^{-1} \text{ cm}^{-1} \text{ s}^{-1}$ . The research demonstrates the importance of side chain engineering of polymeric mixed ionic–electronic conductors in conjunction with their anisotropic microstructural optimization to maximize OECT characteristics.

applications such as transduction/amplification of ionic–electronic signals and the detection of ions and molecules.<sup>[1–4]</sup> The operation principles of OECTs involve ion injection into the active channel by the gate bias and the electrochemical doping of the active channel by electrolyte ions for charge compensation.<sup>[5–11]</sup> To this end, active semiconductors in OECTs need to ensure both ion and electron transport capabilities, and these materials are classified as organic mixed ionic–electronic conductors (OMIECs).<sup>[12–16]</sup> As efficient OMIECs, the conjugated materials grafted with hydrophilic glycol side chains have been successfully demonstrated following poly(3,4-ethylenedioxythiophene):poly(styrene sulfonate) (PEDOT:PSS).<sup>[17,18]</sup> Unlike highly dense inorganic compounds or metal/covalent organic frameworks, glycolated polymers with inherently soft characteristics possess facile ion permeability but simultaneously exhibit imperfect semicrystalline characteristics and disordered fractions in their solid films.<sup>[19,20]</sup>

Thus, to maximize the steady-state performance of OECTs, the enhancement of polymer ordering has been attempted through diverse approaches such as molecular structure optimization,<sup>[21,22]</sup> solvent engineering,<sup>[23,24]</sup> and pre/post-treatments.<sup>[25–27]</sup>

## 1. Introduction

Organic electrochemical transistors (OECTs) have drawn great attention as biocompatible electronics due to their diverse

I.-Y. Jo, Y. Moon, J.-G. Choi, J. H. Kim, D.-Y. Kim, M.-H. Yoon  
School of Materials Science and Engineering  
Gwangju Institute of Science and Technology (GIST)  
Gwangju 61005, Republic of Korea  
E-mail: [mhyoon@gist.ac.kr](mailto:mhyoon@gist.ac.kr)

D. Jeong, S. Lee, B. J. Kim  
Department of Chemical and Biomolecular Engineering  
Korea Advanced Institute of Science and Technology (KAIST)  
Daejeon 34141, Republic of Korea  
E-mail: [bumjoonkim@kaist.ac.kr](mailto:bumjoonkim@kaist.ac.kr)

 The ORCID identification number(s) for the author(s) of this article can be found under <https://doi.org/10.1002/adma.202307402>

DOI: 10.1002/adma.202307402

D. Lee, S. Cho  
Department of Physics and EHSRC  
University of Ulsan  
Ulsan 44610, Republic of Korea

D. Nam, J. Cho  
Department of Chemical and Biological Engineering  
Korea University  
Seoul 02841, Republic of Korea

H. Ahn  
Industrial Technology Convergence Center  
Pohang Accelerator Laboratory  
Pohang University of Science and Technology (POSTECH)  
Pohang 37673, Republic of Korea

In terms of molecular design, extensive structures of conjugated backbones and glycol side chains remain unexplored, suggesting potential for further enhancement of OECT performance. In particular, the side chain engineering in conjugated polymers plays a decisive role in determining the electrical performance by affecting the morphological and energetic ordering of polymers.<sup>[28,29]</sup> First, a side chain structure influences the packing efficiency of the polymer film, which should be secured to develop sufficient charge percolation pathways through well-ordered crystalline phases.<sup>[30]</sup> Moreover, the microstructural ordering of polymers is related to their energetic disorder.<sup>[31,32]</sup> Therefore, highly ordered microstructures of polymer films suppress the formation of trap states, thereby, facilitating charge carrier transport.<sup>[33]</sup> Meanwhile, in addition to molecular optimization, the overall polymer chain alignment along the active channel direction is highly desired to maximize device characteristics. Accordingly, a number of film forming methods have been developed to reinforce polymer packing efficiency and control chain orientation by utilizing mechanical forces<sup>[34,35]</sup> and solution phase alignment.<sup>[36–38]</sup> However, the majority of these techniques have been demonstrated only for conventional polymers with aliphatic side chains, not for conjugated polymers with glycol side chains. This could be attributed to less efficient polymer packing by relatively flexible glycol side chains and the difficulty in selecting an appropriate processing solvent that can induce chain alignment as well as provide sufficient processability for glycolated polymers.<sup>[39]</sup> Therefore, the molecular design rules that can minimize the intrinsic disorders of glycolated polymers and enable film forming methods for the maximization of polymer chain alignment should be established, thereby enhancing steady-state performance and the relevant figure-of-merit of OECTs, the product of charge carrier mobility ( $\mu$ ) and volumetric capacitance ( $C^*$ ).<sup>[40]</sup>

To this end, the side chain structure of glycolated polymers needs to be developed by addressing the following requirements. 1) Since glycol side chains have higher chain flexibility than aliphatic chains, glycol side chains often induce serious microstructural disorders in polymer packing and additional energy tail states that can function as trap states.<sup>[39]</sup> This justifies the use of aliphatic–glycol hybrid side chains, while each fraction should be balanced to ensure not only good polymer ordering by aliphatic moieties but also facile ionic transport by glycol moieties.<sup>[41–43]</sup> 2) The different rigidities of various backbone structures (e.g., thiophene, diketopyrrolopyrrole, naphthalenediimide, and isoindigo) should be considered.<sup>[44–46]</sup> The rigid polymers consisting of multiple fused rings require long and/or branched side chains to enable not only their processing in solution but also sufficient time to construct well-ordered packing structures through polymer self-assembly during solution processing.<sup>[47]</sup> For example, Gao et al. adjusted the side chain structures of diketopyrrolopyrrole (DPP)-based polymers for use in organic field-effect transistors (OFETs), where the polymer with the optimized side chains exhibited improved crystallinity and  $\mu$  value, compared to those with shorter side chains.<sup>[48]</sup> 3) At the same time, the length of side chains should be delicately controlled so as not to be excessively elongated, thereby maintaining the preaggregated state of polymers in solution and, in turn, forming large crystalline domains in film.<sup>[49–51]</sup> In particular, the existence of polymer preaggregates in solution is crucial

for enabling the intentional control of chain orientation by aligning the preaggregates through external mechanical stimuli.<sup>[52,53]</sup> Therefore, through the abovementioned optimization of molecular structures and film forming methods, it is anticipated to realize well-ordered polymer films enabling high device performances.

Herein, we report a series of DPP-based polymeric OMIECs with systematically controlled structures of glycol side chains. The number of ethylene glycol (EG) repeating units is modulated from two to five, thereby, naming the polymer PDPP-*m*EG (where *m* is 2, 3, 4, and 5). Among the polymer series, PDPP-4EG with the medium length of glycol side chains shows the most crystalline and well-ordered characteristics. Thus, PDPP-4EG exhibits the highest OFET saturation hole mobility value and the lowest trap density of states. In parallel, OECT devices are fabricated to investigate the correlation between structural/energetic characteristics and OECT figure-of-merits ( $\mu C^*$ ). In particular, PDPP-4EG enables an excellent  $\mu C^*$  value, which is attributed to its highly optimized charge carrier mobility. Finally, a floating film transfer method is employed to generate the anisotropic alignment of glycolated polymer chains along the active channel direction in OECT devices. The OECT devices based on PDPP-4EG films aligned in a direction parallel or perpendicular to the source-to-drain channel are fabricated to examine the effect of the polymer chain alignment on the resultant  $\mu C^*$  value.

## 2. Results and Discussion

Comprehensive strategies ranging from the molecular design of DPP-based polymers to a film alignment method were employed to minimize the structural and energetic disorders in polymer films and, thus, enhance the resultant OECT steady-state performances (**Figure 1a**). Regarding chemical structures, we introduced hexyl aliphatic spacers between the DPP backbones and the glycol side chains to prevent the latter from hampering the polymer microstructural ordering.<sup>[39]</sup> The length of hexyl spacers was inspired by the branching point of DPP-based polymers that can maximize the polymer crystallinity and the  $\mu$  in OFET devices.<sup>[54]</sup> Additionally, the number of glycol repeating units as side chains was systematically controlled from 2 to 5 in order to analyze their effects on polymer properties. After exploring various backbone spacers, 2,2'-bithiophene (T2) was selected as the optimal structure to produce a high device performance. The synthetic procedures of monomers and corresponding polymers are detailed in the Supporting Information and their chemical structures were confirmed through nuclear magnetic resonance (NMR) analysis (Scheme S1 and Figures S1–S6, Supporting Information). Since the peaks in the <sup>1</sup>H NMR spectra of PDPP-3EG, -4EG, and -5EG polymers were broadened compared to those of PDPP-2EG, the molecular weights (MWs) of PDPP-3EG, -4EG, and -5EG polymers were expected to be higher than that of PDPP-2EG. As similar to previously reported DPP-based polymers,<sup>[55–58]</sup> MWs could not be measured via chloroform- or 1,2,4-trichlorobenzene-based size-exclusion chromatography due to aggregation of polymers and overestimation of MW. Instead, the numbers of repeating units in the polymers were assessed through matrix-assisted laser desorption ionization time-of-flight mass spectrometry (MALDI-ToF MS).

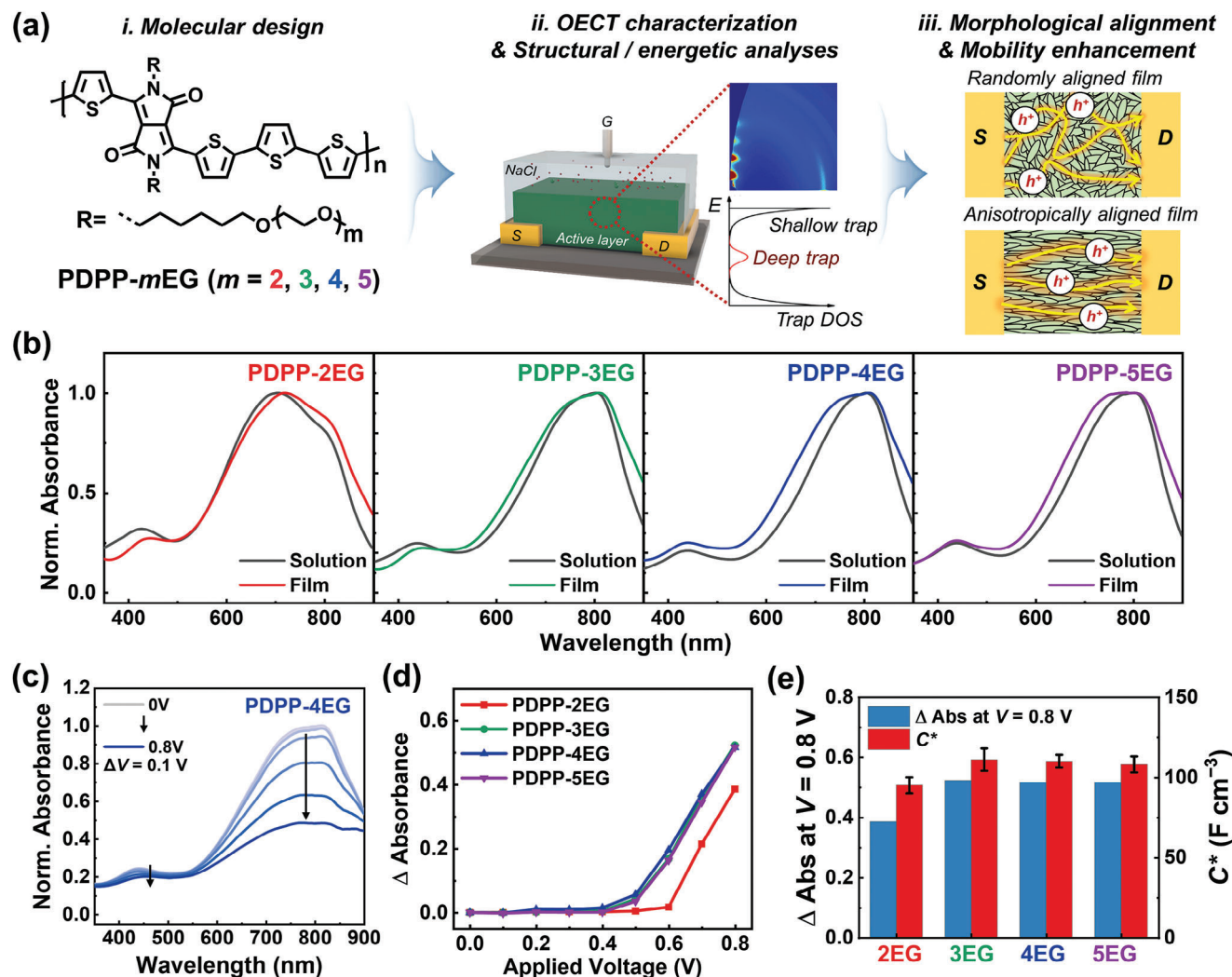


**Figure 1.** a) Chemical structures of the synthesized polymers and schematic illustration of this research; the molecular design rule of the polymers and the method for controlling their chain alignment were investigated to reduce microstructural/energetic disorders and enhance OECT performance. b) Normalized UV-vis absorption spectra of the polymers in solution and film states indicating the preaggregated behaviors of the polymers in solution states. c) Potential-dependent UV-vis absorption spectra of a representative PDPP-4EG polymer film. d) Changes in the absorbance at the maximum absorption wavelength. e) Changes in the maximum absorbance at the applied bias of 0.8 V (blue) and volumetric capacitances (red) of PDPP-mEG.

However, even the MALDI-ToF measurement brought about indecisive results in determining the MWs (Figure S7, Supporting Information), since the high MW parts of polydisperse polymers can be underestimated.<sup>[59]</sup>

The optical property of the polymers was examined using ultraviolet-visible (UV-vis) absorption spectroscopy (Figure 1b). The other three polymers except for PDPP-2EG produced similar absorption spectra in both solution and film states. Meanwhile, PDPP-2EG showed an unsaturated and relatively blue-shifted absorption spectrum probably due to its lower MW, which could be attributed to the short side chains and the resultant low solubility during the synthesis. The PDPP-3EG, -4EG, and -5EG polymers showed similar maximum absorption wavelengths ( $\lambda_{\max}$ s) in both solution and film states,  $\approx 800$  nm (Table 1 and Figure 1b), indicating the preaggregated state of polymer chains in solution.<sup>[60]</sup> Furthermore, the prominent 0–0 vibronic transition peaks were observed in PDPP-3EG, -4EG, and

-5EG polymers, which suggest the presence of *J*-aggregates.<sup>[61,62]</sup> Such anisotropic head-to-tail forms of *J*-aggregates could be transferred to the formation of aligned polymer chains in the

**Table 1.** Optical and electrochemical properties of the polymers.

Polymer	$\lambda_{\max, \text{sol}}$ <sup>a)</sup> [nm]	$\lambda_{\max, \text{film}}$ [nm]	$E_{\text{ox, aq}}$ <sup>b)</sup> [V]	$E_{\text{ox, org}}$ <sup>c)</sup> [V]	IP <sup>d)</sup> [eV]
PDPP-2EG	706	720	0.47	0.15	-5.21
PDPP-3EG	805	810	0.44	0.09	-5.15
PDPP-4EG	805	810	0.42	0.08	-5.14
PDPP-5EG	800	803	0.42	0.06	-5.12

a) Chloroform solution; b) Oxidation onset in a 0.1 M NaCl aqueous electrolyte; c) Oxidation onset in 0.1 M tetrabutylammonium hexafluorophosphate in acetonitrile; d) Calculated from  $\text{IP} = -5.12 \text{ eV} - e(E_{\text{ox, org}} - E_{1/2})$ , where  $E_{1/2}$  is the half-wave potential of a ferrocene/ferrocenium redox couple.

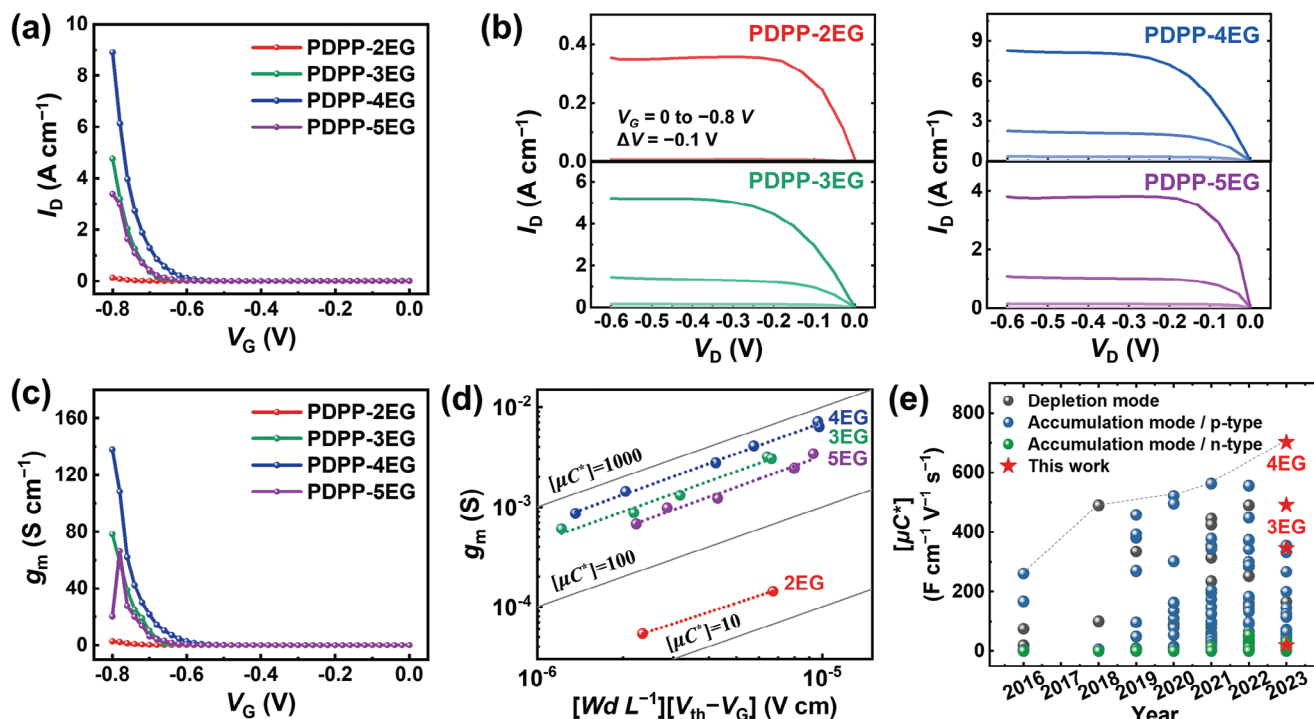


**Figure 2.** Representative geometry-normalized a) transfer, b) output, and c) transconductance curves of OECT devices with 0.1 M NaCl aqueous electrolytes. d)  $g_m$  versus  $(WdL^{-1})(V_{th}-V_G)$  plots. e) Benchmarking of the figure-of-merit  $[\mu C^*]$  values of the polymers reported in the previous literature and this research. For a fair comparison, only the information of OECT devices using NaCl, KCl, or phosphate buffered saline solutions as gate electrolytes were collected.

resultant film when external stimuli such as shear/mechanical forces are applied (vide infra).<sup>[63–65]</sup>

The oxidation onsets in the presence of aqueous ( $E_{ox,aq}$ ) and organic ( $E_{ox,org}$ ) electrolytes and the corresponding ionization potentials (IPs) were evaluated through cyclic voltammetry measurements (Table 1; Figures S8 and S9, Supporting Information). The gradual decreases in  $E_{ox,aq}$  (0.44–0.42 V) and  $E_{ox,org}$  (0.09–0.06 V) values were observed for PDPP-3EG, -4EG, and -5EG polymers, while PDPP-2EG showed relatively high  $E_{ox,aq}$  (0.47 V) and  $E_{ox,org}$  (0.15 V) due to its relatively low MW and broadened bandgap. PDPP-3EG, -4EG, and -5EG displayed neglectable current reduction during five redox cycles in an aqueous electrolyte solution. Furthermore, to investigate ion doping and polymer oxidation behaviors, spectroelectrochemistry was performed using the polymer films immersed in the 0.1 M NaCl aqueous solution (Figure 1c; Figure S10, Supporting Information).<sup>[66–68]</sup> Upon bias, the intensity of both  $\pi-\pi^*$  transition (350–520 nm) and intramolecular charge transfer (ICT) (520–900 nm) peaks were gradually decreased in all polymer films. For quantitative comparison, the change in absorbance was tracked depending on the applied potential at the maximum absorption wavelengths of ICT peaks. Except for PDPP-2EG, the other polymers started to be oxidized at the same potential of 0.5 V and exhibited similar absorbance changes (Figure 1d). On the other hand, PDPP-2EG was oxidized from a higher potential of 0.7 V with less absorbance change. In addition, electrochemical impedance spectroscopy (EIS) was carried out to examine the correlation between electrochemical oxidation behavior and  $C^*$  of each polymer. The corresponding Bode and  $C^*-V$  plots are provided in Figures S11

and S12 of the Supporting Information. Consistent with the result of spectroelectrochemistry, PDPP-3EG, -4EG, and -5EG polymers yielded similar  $C^*$  values of 114, 108, and 108 F cm<sup>-3</sup>, respectively. Meanwhile, PDPP-2EG exhibited a lower  $C^*$  value of 98 F cm<sup>-3</sup> (Figure 1e), which may be ascribed to its lower MW as evidenced by NMR and UV–vis absorption spectra.

To evaluate the electrical/electrochemical characteristics of the polymers, OECT devices were fabricated using a 0.1 M NaCl aqueous electrolyte.<sup>[69]</sup> The active polymers were spin-cast by using chloroform but any pre- or post-treatments were not applied to extract their intrinsic properties. Detailed fabrication procedures are described in the Supporting Information. The representative transfer, output, and transconductance ( $g_m$ ) curves of OECT devices are provided in Figure 2a–c and Figure S13 (Supporting Information). The OECT devices based on PDPP-3EG, -4EG, and -5EG polymers showed on/off drain current ratio ( $I_{on}/I_{off}$ ) values in the range of  $10^5$ – $10^6$  while PDPP-2EG-based devices produced a relatively low  $I_{on}/I_{off}$  of  $10^4$ . The higher  $I_{on}/I_{off}$  values of the OECTs compared to those of the OFETs ( $\approx 10^3$ ; vide infra) were attributed to the doping process by ion injection and the resultant amplified on currents, as evidenced by the above-discussed spectroelectrochemistry and EIS results. Meanwhile, it is noteworthy that  $\mu$  values are the primary determinants that differentiate the performance of OECT devices, considering that there is no significant difference among the  $C^*$  values and doping efficiency of PDPP-3EG, -4EG, and -5EG polymers, except for PDPP-2EG. Among the polymers, PDPP-4EG exhibited the highest drain current ( $I_D$ ) and peak  $g_m$  ( $g_{m,max}$ ) value. To fairly compare material characteristics and exclude the effects of device

**Table 2.** Performance metrics of the OECT devices.

Polymer	$d^a)$ [nm]	$V_{th}$ [V]	$g_{m,norm}^b)$ [S cm <sup>-1</sup> ]	$[\mu C^*]^c)$ [F V <sup>-1</sup> cm <sup>-1</sup> s <sup>-1</sup> ]	$[\mu C^*]^d)$ [F V <sup>-1</sup> cm <sup>-1</sup> s <sup>-1</sup> ]	$\mu_{OECT}^e)$ [cm <sup>2</sup> V <sup>-1</sup> s <sup>-1</sup> ]	$\tau_{on}$ [ms]
PDPP-2EG	127 ± 2	-0.66	1.7 ± 0.3	20	22 ± 1	0.12 ± 0.02	289 ± 24
PDPP-3EG	116 ± 4	-0.61	76.3 ± 5.9	491	466 ± 34	3.95 ± 0.46	160 ± 5
PDPP-4EG	121 ± 5	-0.60	137.1 ± 11.4	702	684 ± 33	6.49 ± 0.60	39 ± 2
PDPP-5EG	128 ± 2	-0.60	63.3 ± 5.6	346	318 ± 29	3.08 ± 0.29	15 ± 1

<sup>a)</sup> Thickness of active channels; <sup>b)</sup> Peak transconductance normalized by active channel geometry ( $WdL^{-1}$ ); <sup>c)</sup> Extracted from the fitting of  $g_m$  versus ( $WdL^{-1})(V_{th}-V_G)$  plots; <sup>d)</sup> Average and standard deviation values from the  $[\mu C^*]$  value of each device; <sup>e)</sup> Calculated by dividing  $[\mu C^*]$  figure-of-merits by  $C^*$  values. The metrics were obtained by averaging at least four devices.

geometry and bias condition,  $[\mu C^*]$  values were extracted from the  $g_m$  versus ( $WdL^{-1})(V_{th}-V_G)$  plots of OECTs with various device geometries (Figure 2d). Intriguingly, PDPP-4EG showed a  $[\mu C^*]$  of 702 F V<sup>-1</sup> cm<sup>-1</sup> s<sup>-1</sup>, which presents a very high value among accumulation-mode OECT materials when comparing the intrinsic performance of materials by excluding the effect of mechanical engineering and molecular weight fractionation (Figure 2e; Figure S14 and Tables S1 and S2, Supporting Information). This  $[\mu C^*]$  value is also higher than those of thermally annealed or acid/ionic liquid-treated PEDOT:PSS films for depletion-mode OECTs (Table S3, Supporting Information). Meanwhile, PDPP-3EG and PDPP-5EG exhibited  $[\mu C^*]$  values of 491 and 346 F V<sup>-1</sup> cm<sup>-1</sup> s<sup>-1</sup>, respectively. By contrast, PDPP-2EG had a sharply decreased  $[\mu C^*]$  of 20 F V<sup>-1</sup> cm<sup>-1</sup> s<sup>-1</sup>, where this phenomenon has been reported for other polymers with very short glycol side chains.<sup>[70,71]</sup> We suppose that the poor performance of PDPP-2EG could be attributed to inferior domain connectivity resulting from its low MW. The PDPP-4EG produced the highest  $\mu_{OECT}$  of 6.49 ± 0.60 cm<sup>2</sup> V<sup>-1</sup> s<sup>-1</sup> and geometry ( $WdL^{-1}$ )-normalized peak gm ( $g_{m,norm}$ ) of 137.1 ± 11.4 S cm<sup>-1</sup>, followed by PDPP-3EG ( $\mu_{OECT} = 3.95 \pm 0.46$  cm<sup>2</sup> V<sup>-1</sup> s<sup>-1</sup>,  $g_{m,norm} = 76.3 \pm 5.9$  S cm<sup>-1</sup>), PDPP-5EG ( $\mu_{OECT} = 3.08 \pm 0.29$  cm<sup>2</sup> V<sup>-1</sup> s<sup>-1</sup>,  $g_{m,norm} = 63.3 \pm 5.6$  S cm<sup>-1</sup>), and PDPP-2EG ( $\mu_{OECT} = 0.12 \pm 0.02$  cm<sup>2</sup> V<sup>-1</sup> s<sup>-1</sup>,  $g_{m,norm} = 1.7 \pm 0.3$  S cm<sup>-1</sup>).

In addition to steady-state device performance, transient characteristics are also important for rapid response to ion/molecule signals. Therefore, the transient performance of OECT devices was evaluated by time constants upon switching on ( $\tau_{on}$ ) (Table 2; Figure S15, Supporting Information).  $\tau_{on}$  values significantly decreased from 289 ± 24 ms (PDPP-2EG) and 160 ± 5 ms (PDPP-3EG) to 39 ± 2 ms (PDPP-4EG) and 15 ± 1 ms (PDPP-5EG). Overall, both PDPP-4EG and PDPP-5EG exhibited fast responses to gate bias, owing to facilitated ion transport through relatively long glycol side chains. Furthermore, operational stability tests were performed by turning OECT devices on ( $V_G = -0.7$  V) and off ( $V_G = 0.0$  V) repeatedly for a duration of 1.5 h (Figure S16, Supporting Information). Interestingly, PDPP-3EG and -4EG devices maintained 99% and 88% of the initial on-currents, respectively, while PDPP-2EG and -5EG devices retained only 28% and 33% of the initial on-currents, respectively. These results could be attributed to the morphological degradation in the films due to the relatively low molecular weight of PDPP-2EG and the high swelling degree of PDPP-5EG, respectively.

To evaluate the electrical characteristics of the polymers independent of swelling and ion-mediated doping, bottom-gate top-

contact OFET devices were also fabricated, where 200 nm-thick SiO<sub>2</sub> served as a gate dielectric with a capacitance of 17.3 nF cm<sup>-2</sup>. The detailed procedures for OFET device fabrication and electrical characterization are provided in the Supporting Information. The representative transfer curves and the corresponding transistor mobility ( $\mu_{OFET}$ ) at the saturation regime are presented in Figure 3a and Table 3. The OFETs based on PDPP-3EG, -4EG, and -5EG polymers exhibited  $I_{on}/I_{off}$  values exceeding 10<sup>3</sup>. In agreement with OECT results, PDPP-4EG showed the highest  $\mu_{OFET}$  of 4.0 × 10<sup>-2</sup> cm<sup>2</sup> V<sup>-1</sup> s<sup>-1</sup>, while PDPP-2EG, -3EG, and -5EG polymers exhibited relatively lower  $\mu_{OFET}$  values of 4.0 × 10<sup>-3</sup>, 3.1 × 10<sup>-2</sup>, and 2.0 × 10<sup>-2</sup> cm<sup>2</sup> V<sup>-1</sup> s<sup>-1</sup>, respectively. In parallel, to investigate the energetic disorder in polymer films, subthreshold swing ( $S_g$ ) values and the corresponding number of interface trap states ( $N_{it}$ ) were calculated (Figure 3b and Table 3), as the change of electrical current in the subthreshold regime is dependent on the presence of trap states as well as charge carrier density determined by the applied electric field.<sup>[72]</sup> In comparison with PDPP-2EG (19.2 V dec<sup>-1</sup>), PDPP-5EG (11.1 V dec<sup>-1</sup>), and PDPP-3EG (9.3 V dec<sup>-1</sup>), PDPP-4EG exhibits a low  $S_g$  value of 7.1 V dec<sup>-1</sup>, resulting in the lowest  $N_{it}$  value of 1.3 × 10<sup>13</sup> eV<sup>-1</sup> cm<sup>-2</sup>.

To further quantify trap states in polymer films, thermal admittance spectroscopy (TAS) was performed to obtain the energetic profiles of trap density of states (tDOS) (Figure 3c).<sup>[73,74]</sup> The device fabrication process and the derivation of tDOS values are detailed in the Supporting Information. In a low energy depth of 0.25–0.4 eV, PDPP-3EG and -4EG showed suppressed energetic disorders with similarly low tDOS of 6.2 × 10<sup>15</sup> and 5.8 × 10<sup>15</sup> cm<sup>-3</sup>, respectively (Figure 3d and Table 3), whereas PDPP-2EG and PDPP-5EG exhibited relatively high tDOS values of 4.2 × 10<sup>18</sup> and 2.2 × 10<sup>17</sup> cm<sup>-3</sup>, respectively. Interestingly, the discrepancies in the tDOS of the polymers became more distinct in a higher energy depth of 0.4–0.5 eV, as exemplified by the lowest tDOS value of PDPP-4EG (3.3 × 10<sup>17</sup> cm<sup>-3</sup>). Therefore, PDPP-4EG featured the lowest degree of energetic disorder in the family, which is clearly reflected in its OFET and OECT device characteristics.

To disclose the origin of the difference in device performances and energetic disorders of PDPP-*m*EG, the microstructures of oxidized polymer films were investigated through ex situ 2D grazing-incidence X-ray scattering (2D GIXS) analysis. Considering that ion-induced microstructural deformation upon doping/dedoping is not negligible, it is important to interpret the oxidized polymer morphology that can directly replicate the on-state OECT channel. The GIXS line-cut profiles and the corresponding images are provided in Figure 4a,b and Figure S17 (Supporting Information). All the polymers formed highly edge-on

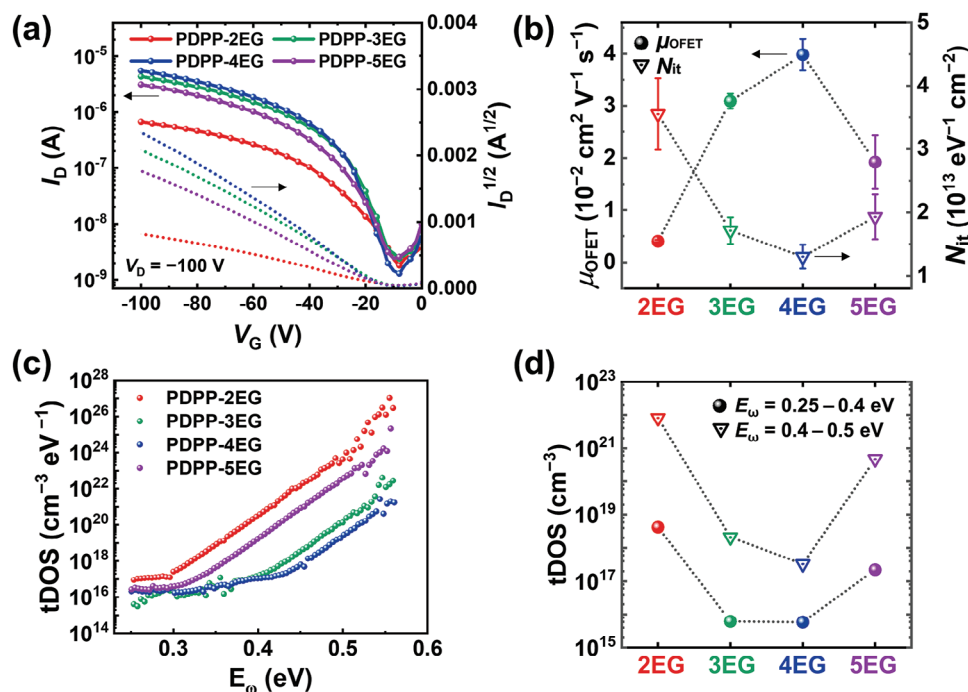


**Figure 3.** a) Representative OFET transfer curves. b) Comparison of the saturation mobility and the number of trap states of the polymer series. c) tDOS spectra of devices based on the polymer series. d) Comparison of the trap density of states depending on trap depths.

**Table 3.** Electrical properties in the OFET devices and trap density of states of the polymer series.

Polymer	$\mu_{\text{OFET}}^{\text{a}}$ [cm <sup>2</sup> V <sup>-1</sup> s <sup>-1</sup> ]	$S_{\text{S}}^{\text{b}}$ [V dec <sup>-1</sup> ]	$N_{\text{tr}}^{\text{b}}$ [10 <sup>13</sup> eV <sup>-1</sup> cm <sup>-2</sup> ]	tDOS <sub>&lt;0.4 eV</sub> <sup>c</sup> [cm <sup>-3</sup> ]	tDOS <sub>&gt;0.4 eV</sub> <sup>d</sup> [cm <sup>-3</sup> ]
PDPP-2EG	$(4.0 \pm 0.2) \times 10^{-3}$	$19.2 \pm 3.0$	$3.6 \pm 0.6$	$4.2 \times 10^{18}$	$8.2 \times 10^{21}$
PDPP-3EG	$(3.1 \pm 0.1) \times 10^{-2}$	$9.3 \pm 1.1$	$1.7 \pm 0.2$	$6.2 \times 10^{15}$	$2.1 \times 10^{18}$
PDPP-4EG	$(4.0 \pm 0.3) \times 10^{-2}$	$7.1 \pm 1.0$	$1.3 \pm 0.2$	$5.8 \times 10^{15}$	$3.3 \times 10^{17}$
PDPP-5EG	$(2.0 \pm 0.5) \times 10^{-2}$	$11.1 \pm 1.9$	$2.0 \pm 0.3$	$2.2 \times 10^{17}$	$4.7 \times 10^{20}$

<sup>a)</sup> Saturation hole mobility averaged over at least five OFET devices; <sup>b)</sup> Average values over at least five OFET devices; <sup>c)</sup> Trap density of states where the energy depth of traps is from 0.25 to 0.4 eV; <sup>d)</sup> Trap density of states where the energy depth of traps is from 0.4 to 0.5 eV.

oriented packing, as evidenced by highly ordered lamellar stacking in the out-of-plane direction and  $\pi$ - $\pi$  stacking in the in-plane direction. PDPP-3EG and -4EG featured higher fourth-order lamellar peaks than PDPP-2EG and -5EG, which showed up to third-order lamellar peaks. For quantitative comparison, the crystal coherence lengths ( $L_c$ ) and paracrystalline disorder parameters ( $g$ ) of (100) lamellar peaks were estimated, which are summarized in Table 4.<sup>[75]</sup> PDPP-4EG exhibited the strongest crystalline properties with an  $L_{c,100}$  of  $11.7 \pm 0.4$  nm, which is higher than those of PDPP-2EG ( $5.9 \pm 0.2$  nm), -3EG ( $8.2 \pm 0.3$  nm), and -5EG ( $10.5 \pm 0.5$  nm) (Figure 4c). In addition, PDPP-4EG produced the lowest  $g_{100}$  ( $16.0 \pm 0.3\%$ ) value when compared to PDPP-2EG ( $20.8 \pm 0.4\%$ ), PDPP-3EG ( $18.3 \pm 0.3\%$ ), and PDPP-5EG ( $17.6 \pm 0.4\%$ ) (Figure 4d). In the case of (010)  $\pi$ - $\pi$  stacking peaks, there were negligible differences in the  $L_c$  and  $g$ -values of the polymer series (Table S4, Supporting Information). From these results, it can be concluded that PDPP-4EG film had well-developed crystalline domains with the lowest microstructural disorder among the PDPP-*m*EG family, which are beneficial

for suppressing energetic disorder and facilitating charge carrier transport as demonstrated by the results shown in TAS and transistor analyses. Consistent with the abovementioned results in an oxidized state, the same trend in crystalline properties was observed in a neat state without ion injection (Figure S18, Supporting Information). The PDPP-4EG exhibited the highest  $L_{c,100}$  of  $11.7 \pm 0.4$  nm and the lowest  $g_{100}$  of  $16.0 \pm 0.3\%$  among the polymer series.

To further compare the crystalline properties of the polymers, differential scanning calorimetry (DSC) analysis was performed during the first heating cycle (Figure 4e). To directly correlate with the polymer morphologies in transistor devices, polymer films were prepared by spin-coating their chloroform solutions identical to those in device fabrication and collected into DSC pans for the measurements.<sup>[76]</sup> Interestingly, endothermic melting transitions appeared in PDPP-4EG and -5EG, whereas exothermic cold crystallization transitions were found in PDPP-2EG and -3EG. The cold crystallization peaks of PDPP-2EG and -3EG indicate the existence of imperfectly crystallized polymers. This

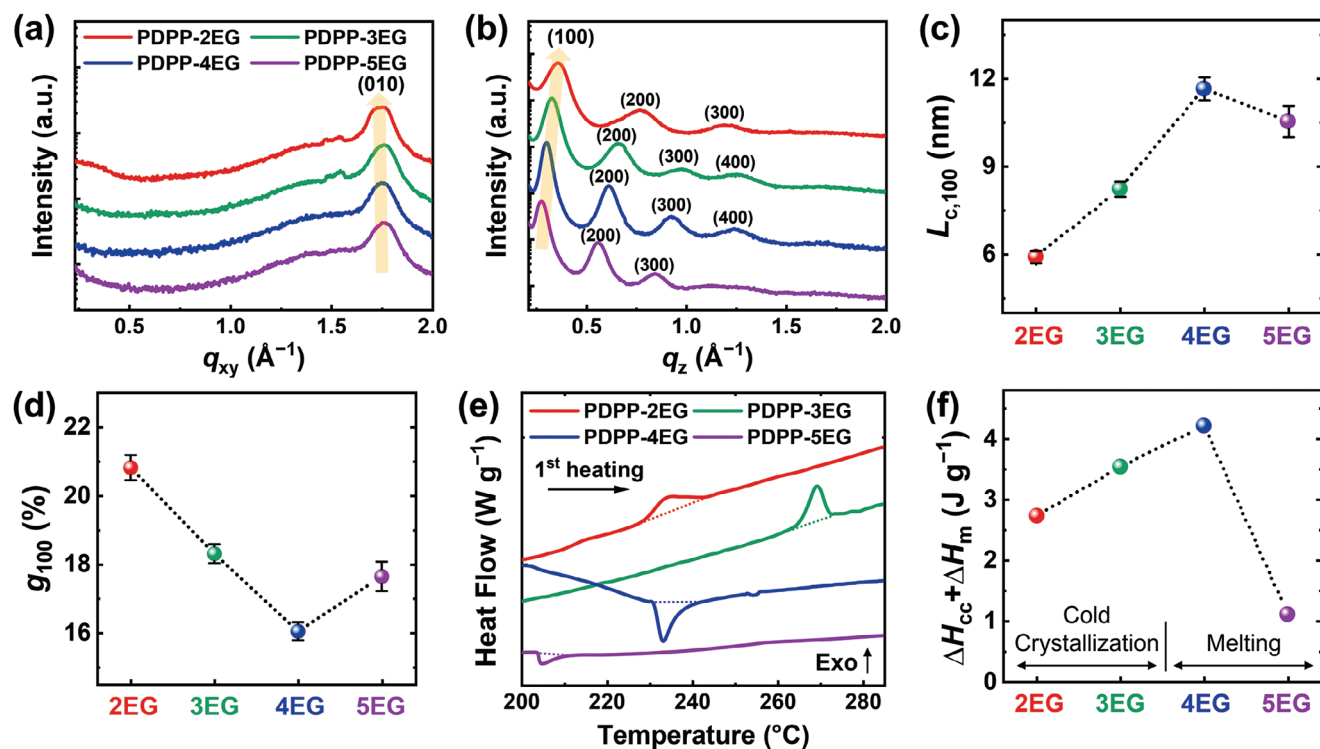


**Figure 4.** GIXS line-cut profiles of the oxidized polymer films in the a) in-plane and b) out-of-plane directions. Plots of c) the coherence lengths and d) the paracrystalline disorder parameters of PDPP-*m*EG polymers from (100) scattering peaks, which were averaged from at least three different films for each polymer. e) DSC thermograms of the polymers during the first heating cycle. The dashed lines signify the integrated regions for the calculation of phase transition enthalpies. f) Comparison of the cold crystallization enthalpies and melting enthalpies of the polymers.

result suggests that the crystallization of the polymers was suppressed during the film formation due to the kinetic reason associated with the low solubilities of the polymers that cause fast precipitation.<sup>[77,78]</sup> By contrast, PDPP-4EG and -5EG could produce well-developed crystalline structures owing to their long side chains. To quantitatively compare the amounts of crystalline phases, the sum of melting enthalpy ( $\Delta H_m$ ) and cold crystallization enthalpy ( $\Delta H_{cc}$ ) was calculated. PDPP-4EG exhibited the highest enthalpy of  $4.2 \text{ J g}^{-1}$ , followed by those of PDPP-3EG ( $3.5 \text{ J g}^{-1}$ ), PDPP-2EG ( $2.7 \text{ J g}^{-1}$ ), and PDPP-5EG ( $1.1 \text{ J g}^{-1}$ ) (Figure 4f and Table 4). Taking into account the GIXS and DSC results, the PDPP-4EG film contained the most strongly developed crystalline structures that are beneficial to reducing energetic disorder and obtaining a high  $\mu$  value.<sup>[48]</sup>

Since the ideal polymer film microstructure for an OECT channel cannot be achieved solely through molecular design, it is highly desired to induce additional chain alignment along the OECT channel. To this end, a unidirectional floating film transfer method (UFTM) was employed to induce anisotropic chain alignment in PDPP-4EG films (Figure S19, Supporting Information).<sup>[79,80]</sup> It is noted again that the preaggregation of PDPP-4EG in chloroform is advantageous to form readily aligned polymer chains (*J*-aggregates) in the solution phase (Figure 1b). As the preaggregated polymer solution was released onto the viscous hydrophilic liquid, the polymer chains underwent unidirectional compression due to a viscous drag force (see the Experimental Section in the Supporting information for details).<sup>[81]</sup> By film transfer, the parallel alignment of poly-

mer backbones could be preserved in solid films. The resultant anisotropic morphology of transferred polymer films could be effective for charge carrier transport along the active channel direction compared to randomly oriented spin-cast polymer films (Figure 5a).

To verify the polymer chain alignment, UV-vis absorption spectroscopy was performed under optical polarizers. When the polarizer was placed in parallel with polymer backbone orientation, the UFTM PDPP-4EG film showed higher absorbance than in the case of perpendicular orientation (Figure 5b). The dichroic ratio and the corresponding 2D order parameter were 1.9 and 0.31, respectively. Consistently, polarized optical microscopy exhibited the anisotropic polymer chain alignment in transferred films (Figure S20, Supporting Information). To investigate the anisotropy of film morphology at a smaller scale,

**Table 4.** Crystalline characteristics of the polymers.

Polymer	$L_{c,100}$ <sup>a)</sup> [nm]	$g_{100}$ [%]	$\Delta H_{cc}$ <sup>b)</sup> [ $\text{J g}^{-1}$ ]	$\Delta H_m$ <sup>b)</sup> [ $\text{J g}^{-1}$ ]
PDPP-2EG	$5.9 \pm 0.2$	$20.8 \pm 0.4$	2.7	–
PDPP-3EG	$8.2 \pm 0.3$	$18.3 \pm 0.3$	3.5	–
PDPP-4EG	$11.7 \pm 0.4$	$16.0 \pm 0.3$	–	4.2
PDPP-5EG	$10.5 \pm 0.5$	$17.6 \pm 0.4$	–	1.1

<sup>a)</sup> Extracted from GIXS line-cut profiles of the oxidized polymer films. Averaged from at least three different films for each polymer; <sup>b)</sup> Obtained from DSC thermograms.

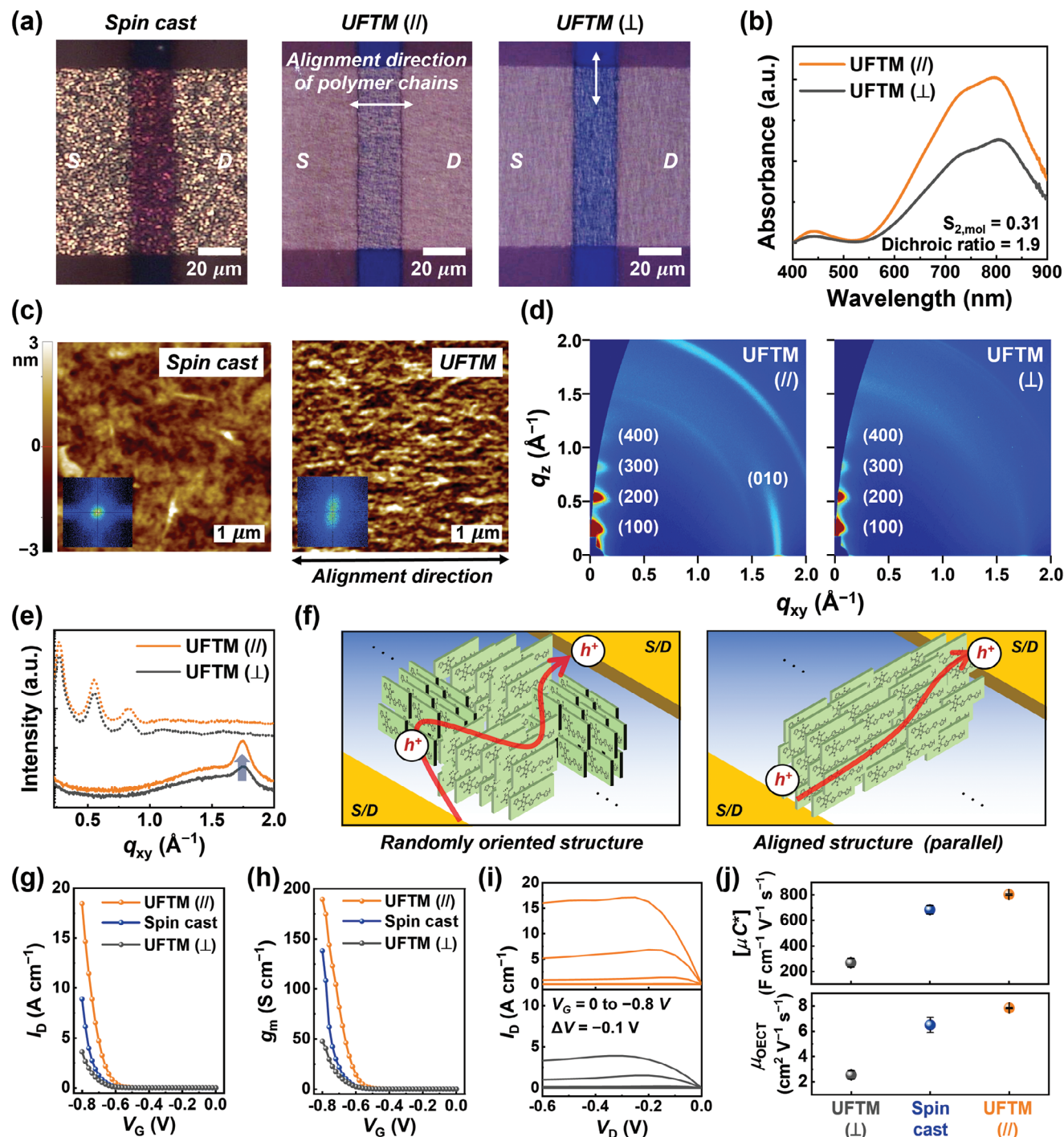


**Figure 5.** a) Optical photographs of PDPP-4EG-based active channels prepared by spin-casting (left) and UFTM (parallel; middle, perpendicular; right). b) UV-vis absorption spectra of transferred PDPP-4EG films with a polarizer in parallel (orange) and perpendicular (gray) to the source–drain channel direction. c) AFM topography images of spin-cast (left) and UFTM (right) PDPP-4EG films with the corresponding FFT-processed images (inset). d) 2D GIXS patterns and e) corresponding line-cut profiles of PDPP-4EG films prepared by UFTM (parallel and perpendicular). f) Schematics of polymer chain alignment in active channels prepared by spin-casting (left) and UFTM (parallel; right). Geometry-normalized g) transfer, h) transconductance, and i) output curves of the OECTs based on PDPP-4EG films prepared by UFTM (parallel; orange), spin-casting (blue), and UFTM (perpendicular; gray). j) Comparison of  $[\mu C^*]$  and  $\mu_{OECT}$  values extracted from PDPP-4EG films prepared by UFTM (parallel; orange), spin-casting (blue), and UFTM (perpendicular; gray).

**Table 5.** Characteristics of OECT devices based on PDPP-4EG films prepared by the UFTM method (parallel vs perpendicular).

Direction	$g_{m, \text{norm}}^{\text{a)}}$ [S cm <sup>-1</sup> ]	$[\mu C^*]^{\text{b)}}$ [F V <sup>-1</sup> cm <sup>-1</sup> s <sup>-1</sup> ]	$\mu_{\text{OECT}}^{\text{c)}}$ [cm <sup>2</sup> V <sup>-1</sup> s <sup>-1</sup> ]	$C^*$ [F cm <sup>-3</sup> ]
Parallel	169.9 ± 7.4	804 ± 7	7.83 ± 0.05	103 ± 3
Perpendicular	51.8 ± 6.6	267 ± 34	2.55 ± 0.33	

<sup>a)</sup> Peak transconductance normalized by active channel geometry ( $WdL^{-1}$ ); <sup>b)</sup> Extracted from the fitting of  $g_m$  versus  $(WdL^{-1})(V_{\text{th}} - V_G)$  plots; <sup>c)</sup> Calculated by dividing  $[\mu C^*]$  figure-of-merits by  $C^*$  values. The values were obtained by averaging at least five devices.

atomic force microscopy (AFM) and GIXS were performed. In contrast to isotropic spin-cast films, PDPP-4EG films transferred by the UFTM process showed anisotropic chain alignment in the AFM images which was also confirmed by the corresponding fast Fourier transform (FFT)-processed AFM images (Figure 5c). In addition, the GIXS result obtained in the parallel direction to polymer backbone orientation exhibited a higher intensity of (010)  $\pi$ - $\pi$  stacking peak than that in the perpendicular direction (Figure 5d,e). As depicted in Figure S21 of the Supporting Information, the parallel alignment of polymer backbones is beneficial for lateral intrachain charge transport between source and drain electrodes in OECT devices.<sup>[82]</sup> It is noted that a similar tendency was reported in the previous literature where the intensity of in-plane (010) stacking for unidirectionally aligned backbones was weakened in perpendicular films.<sup>[83]</sup> As illustrated in Figure 5f, it is expected that the polymer films where polymer backbones are aligned in parallel to the source/drain electrodes should exhibit more efficient charge transport than those with random chain orientations originated by spin-casting.

For a fair comparison, OECT devices comprising PDPP-4EG films prepared by UFTM were fabricated using the same conditions (e.g., polymer solution preparation and device dimensions) as those based on spin-cast PDPP-4EG films. The OECTs based on UFTM PDPP-4EG films aligned with the parallel directionality yielded a very high figure-of-merit  $[\mu C^*]$  of  $804 \pm 7 \text{ F V}^{-1} \text{ cm}^{-1} \text{ s}^{-1}$  and a  $g_{m, \text{norm}}$  of  $169.9 \pm 7.4 \text{ S cm}^{-1}$ , which were approximately fourfold larger than those in the perpendicular direction (Figure 5g-j and Table 5). This suggests that intrachain charge transfer along polymer backbones in the parallel direction is much more effective than interchain charge transfer through adjacent  $\pi$ - $\pi$  stackings in the perpendicular direction. Note that the average  $C^*$  value of UFTM films ( $103 \pm 3 \text{ F cm}^{-3}$ ) was very close to that of spin-cast films ( $107 \pm 4 \text{ F cm}^{-3}$ ) since the  $C^*$  is not sensitive to the change in polymer film crystallinity or morphology (Figure S22, Supporting Information).<sup>[84]</sup> Therefore, compared with spin-cast films, the improvement in the  $[\mu C^*]$  value of OECTs based on UFTM PDPP-4EG films mainly originated from the enhanced  $\mu_{\text{OECT}}$  values ( $7.83 \pm 0.05$  vs  $6.49 \pm 0.60 \text{ cm}^2 \text{ V}^{-1} \text{ s}^{-1}$ ). This result implies the necessity of controlling polymer orientation and lowering microstructural disorders through unidirectional film alignment techniques and their potential to maximize OECT performances. Regarding the optimal UFTM condition, various factors such as the types and temperature of liquid substrates and processing solvents need to be further controlled which is, however, out of scope in this work.

### 3. Conclusions

We have developed a series of DPP-based polymers containing aliphatic-glycol hybrid side chains, where the length of the aliphatic chain is fixed as hexyl and the number of EG repeating units is systematically controlled from two to five. The polymer series except PDPP-2EG exhibited similar electrochemical properties and  $C^*$  values due to the same backbone. Meanwhile, PDPP-4EG featured the most enhanced microstructural ordering and well-developed crystalline domains, as revealed by DSC and GIXS results. In addition, PDPP-4EG exhibited the highest  $\mu_{\text{OFET}}$  value in OFET devices and afforded the lowest tDOS, indicating the most suppressed energetic disorder of PDPP-4EG. The beneficial properties of PDPP-4EG resulted in fast electronic transport in OECTs, thereby producing a  $\mu_{\text{OECT}}$  of  $6.49 \pm 0.60 \text{ cm}^2 \text{ V}^{-1} \text{ s}^{-1}$  and a  $[\mu C^*]$  figure-of-merit of  $702 \text{ F V}^{-1} \text{ cm}^{-1} \text{ s}^{-1}$ . In addition to the optimal molecular design, a unidirectional film alignment technique has been first applied to fabricate the active channels of OECTs to control the packing orientation with respect to the channel direction. Through UFTM, anisotropic and less-disordered crystalline domains were obtained, enabling an even higher  $[\mu C^*]$  value over  $800 \text{ F V}^{-1} \text{ cm}^{-1} \text{ s}^{-1}$ . This study highlights the importance of delicate side chain engineering of OMIECs and chain alignment techniques to realize OECTs with exceptionally high steady-state performance.

### Supporting Information

Supporting Information is available from the Wiley Online Library or from the author.

### Acknowledgements

I.-Y.J. and D.J. contributed equally to this work. This work was supported by the National Research Foundation (NRF) grant funded by the Korean government (MSIT) (RS-2023-00217884, NRF-2021M3H4A1A01004332, NRF-2021R1A2C1013015, and NRF-2021R1A4A1022920).

### Conflict of Interest

The authors declare no conflict of interest.

### Data Availability Statement

Research data are not shared.

### Keywords

high crystallinity, low energetic disorder, mixed ionic-electronic conductors, organic electrochemical transistors, side chain engineering

Received: July 25, 2023  
Revised: November 15, 2023  
Published online: December 4, 2023

- [1] W. Huang, J. Chen, Y. Yao, D. Zheng, X. Ji, L.-W. Feng, D. Moore, N. R. Glavin, M. Xie, Y. Chen, R. M. Pankow, A. Surendran, Z. Wang, Y. Xia, L. Bai, J. Rivnay, J. Ping, X. Guo, Y. Cheng, T. J. Marks, A. Facchetti, *Nature* **2023**, 613, 496.

- [2] P. Romele, P. Gkoupidenis, D. A. Koutsouras, K. Lieberth, Z. M. Kovács-Vajna, P. W. M. Blom, F. Torricelli, *Nat. Commun.* **2020**, *11*, 3743.
- [3] J. Song, G. Tang, J. Cao, H. Liu, Z. Zhao, S. Griggs, A. Yang, N. Wang, H. Cheng, C.-K. Liu, I. Mcculloch, F. Yan, *Adv. Mater.* **2023**, *35*, 2207763.
- [4] M. Wu, K. Yao, N. Huang, H. Li, J. Zhou, R. Shi, J. Li, X. Huang, J. Li, H. Jia, Z. Gao, T. H. Wong, D. Li, S. Hou, Y. Liu, S. Zhang, E. Song, J. Yu, X. Yu, *Adv. Sci.* **2023**, *10*, 2300504.
- [5] S. H. Kim, K. Hong, W. Xie, K. H. Lee, S. Zhang, T. P. Lodge, C. D. Frisbie, *Adv. Mater.* **2013**, *25*, 1822.
- [6] J. Rivnay, S. Inal, A. Salleo, R. M. Owens, M. Berggren, G. G. Malliaras, *Nat. Rev. Mater.* **2018**, *3*, 17086.
- [7] C. G. Bischak, L. Q. Flagg, D. S. Ginger, *Adv. Mater.* **2020**, *32*, 2002610.
- [8] V. Kaphle, P. R. Paudel, D. Dahal, R. K. Radha Krishnan, B. Lüssem, *Nat. Commun.* **2020**, *11*, 2515.
- [9] M. Cucchi, A. Weissbach, L. M. Bongartz, R. Kantelberg, H. Tseng, H. Kleemann, K. Leo, *Nat. Commun.* **2022**, *13*, 4514.
- [10] Y. Kim, G. Kim, B. Ding, D. Jeong, I. Lee, S. Park, B. J. Kim, I. Mcculloch, M. Heeney, M.-H. Yoon, *Adv. Mater.* **2022**, *34*, 2107355.
- [11] P. Cavassin, I. Holzer, D. Tsokkou, O. Bardagot, J. Réhault, N. Banerji, *Adv. Mater.* **2023**, *35*, 2300308.
- [12] E. Zeglio, O. Inganäs, *Adv. Mater.* **2018**, *30*, 1800941.
- [13] B. D. Paulsen, K. Tybrandt, E. Stavrinidou, J. Rivnay, *Nat. Mater.* **2020**, *19*, 13.
- [14] J. H. Kim, S.-M. Kim, G. Kim, M.-H. Yoon, *Macromol. Biosci.* **2020**, *20*, 2000211.
- [15] L. Zhang, S. Khayour, G. Ren, S. He, J. Wang, L. Yu, Y. Song, C. Zhu, X. Kang, Y. Zhang, Z. Gong, K. Gao, J. Wang, H. Sheng, G. Lu, H.-D. Yu, *J. Mater. Chem. C* **2023**, *11*, 7272.
- [16] P. C. Harikesh, C.-Y. Yang, H.-Y. Wu, S. Zhang, M. J. Donahue, A. S. Caravaca, J.-D. Huang, P. S. Olofsson, M. Berggren, D. Tu, S. Fabiano, *Nat. Mater.* **2023**, *22*, 242.
- [17] C. B. Nielsen, A. Giovannitti, D.-T. Sbircea, E. Bandiello, M. R. Niazi, D. A. Hanifi, M. Sessolo, A. Amassian, G. G. Malliaras, J. Rivnay, I. Mcculloch, *J. Am. Chem. Soc.* **2016**, *138*, 10252.
- [18] A. Giovannitti, C. B. Nielsen, D.-T. Sbircea, S. Inal, M. Donahue, M. R. Niazi, D. A. Hanifi, A. Amassian, G. G. Malliaras, J. Rivnay, I. Mcculloch, *Nat. Commun.* **2016**, *7*, 13066.
- [19] Z. Peng, L. Ye, H. Ade, *Mater. Horiz.* **2022**, *9*, 577.
- [20] J. Song, H. Liu, Z. Zhao, X. Guo, C.-K. Liu, S. Griggs, A. Marks, Y. Zhu, H. K.-W. Law, I. Mcculloch, F. Yan, *Sci. Adv.* **2023**, *9*, 9627.
- [21] P. Schmode, A. Savva, R. Kahl, D. Ohayon, F. Meichsner, O. Dolynchuk, T. Thurn-Albrecht, S. Inal, M. Thelakkt, *ACS Appl. Mater. Interfaces* **2020**, *12*, 13029.
- [22] Z. S. Parr, J. Borges-González, R. B. Rashid, K. J. Thorley, D. Meli, B. D. Paulsen, J. Strzalka, J. Rivnay, C. B. Nielsen, *Adv. Mater.* **2022**, *34*, 2107829.
- [23] A. Savva, D. Ohayon, J. Surgailis, A. F. Paterson, T. C. Hidalgo, X. Chen, I. P. Maria, B. D. Paulsen, A. J. Petty II, J. Rivnay, I. Mcculloch, S. Inal, *Adv. Electron. Mater.* **2019**, *5*, 1900249.
- [24] G. Zhu, J. Chen, J. Duan, H. Liao, X. Zhu, Z. Li, I. Mcculloch, W. Yue, *ACS Appl. Mater. Interfaces* **2022**, *14*, 43586.
- [25] K. Feng, W. Shan, S. Ma, Z. Wu, J. Chen, H. Guo, B. Liu, J. Wang, B. Li, H. Y. Woo, S. Fabiano, W. Huang, X. Guo, *Angew. Chem., Int. Ed.* **2021**, *60*, 24198.
- [26] E. Tan, J. Kim, K. Stewart, C. Pitsalidis, S. Kwon, N. Siemons, J. Kim, Y. Jiang, J. M. Frost, D. Pearce, J. E. Tyrrell, J. Nelson, R. M. Owens, Y.-H. Kim, J.-S. Kim, *Adv. Mater.* **2022**, *34*, 2202574.
- [27] K. Feng, W. Shan, J. Wang, J.-W. Lee, W. Yang, W. Wu, Y. Wang, B. J. Kim, X. Guo, H. Guo, *Adv. Mater.* **2022**, *34*, 2201340.
- [28] N. A. Kukhta, A. Marks, C. K. Luscombe, *Chem. Rev.* **2022**, *122*, 4325.
- [29] M. Moser, Y. Wang, T. C. Hidalgo, H. Liao, Y. Yu, J. Chen, J. Duan, F. Moruzzi, S. Griggs, A. Marks, N. Gasparini, A. Wadsworth, S. Inal, I. Mcculloch, W. Yue, *Mater. Horiz.* **2022**, *9*, 973.
- [30] J.-W. Lee, N. Choi, D. Kim, T. N.-L. Phan, H. Kang, T.-S. Kim, B. J. Kim, *Chem. Mater.* **2021**, *33*, 1070.
- [31] X. Yan, M. Xiong, X.-Y. Deng, K.-K. Liu, J.-T. Li, X.-Q. Wang, S. Zhang, N. Prine, Z. Zhang, W. Huang, Y. Wang, J.-Y. Wang, X. Gu, S. K. So, J. Zhu, T. Lei, *Nat. Commun.* **2021**, *12*, 5723.
- [32] D. Venkateshvaran, M. Nikolka, A. Sadhanala, V. Lemaure, M. Zelazny, M. Kepa, M. Hurhangee, A. J. Kronemeijer, V. Pecunia, I. Nasrallah, I. Romanov, K. Broch, I. Mcculloch, D. Emin, Y. Olivier, J. Cornil, D. Beljonne, H. Sirringhaus, *Nature* **2014**, *515*, 384.
- [33] R. Noriega, J. Rivnay, K. Vandewal, F. P. V. Koch, N. Stingelin, P. Smith, M. F. Toney, A. Salleo, *Nat. Mater.* **2013**, *12*, 1038.
- [34] B. O'connor, R. J. Kline, B. R. Conrad, L. J. Richter, D. Gundlach, M. F. Toney, D. M. Delongchamp, *Adv. Funct. Mater.* **2011**, *21*, 3697.
- [35] L. Hartmann, K. Tremel, S. Uttiya, E. Crossland, S. Ludwigs, N. Kayunkid, C. Vergnat, M. Brinkmann, *Adv. Funct. Mater.* **2011**, *21*, 4047.
- [36] J. Soeda, H. Matsui, T. Okamoto, I. Osaka, K. Takimiya, J. Takeya, *Adv. Mater.* **2014**, *26*, 6430.
- [37] Y. Jiang, J. Chen, Y. Sun, Q. Li, Z. Cai, J. Li, Y. Guo, W. Hu, Y. Liu, *Adv. Mater.* **2019**, *31*, 1805761.
- [38] J. Shin, T. R. Hong, T. W. Lee, A. Kim, Y. H. Kim, M. J. Cho, D. H. Choi, *Adv. Mater.* **2014**, *26*, 6031.
- [39] R. Kim, B. Kang, D. H. Sin, H. H. Choi, S.-K. Kwon, Y.-H. Kim, K. Cho, *Chem. Commun.* **2015**, *51*, 1524.
- [40] S. Inal, G. G. Malliaras, J. Rivnay, *Nat. Commun.* **2017**, *8*, 1767.
- [41] A. Savva, R. Hallani, C. Cendra, J. Surgailis, T. C. Hidalgo, S. Wustoni, R. Sheelamanthula, X. Chen, M. Kirkus, A. Giovannitti, A. Salleo, I. Mcculloch, S. Inal, *Adv. Funct. Mater.* **2020**, *30*, 1907657.
- [42] S. E. Chen, L. Q. Flagg, J. W. Onorato, L. J. Richter, J. Guo, C. K. Luscombe, D. S. Ginger, *J. Mater. Chem. A* **2022**, *10*, 10738.
- [43] A. A. Szumska, I. P. Maria, L. Q. Flagg, A. Savva, J. Surgailis, B. D. Paulsen, D. Moia, X. Chen, S. Griggs, J. T. Mefford, R. B. Rashid, A. Marks, S. Inal, D. S. Ginger, A. Giovannitti, J. Nelson, *J. Am. Chem. Soc.* **2021**, *143*, 14795.
- [44] C. Lee, H. R. Lee, J. Choi, Y. Kim, T. L. Nguyen, W. Lee, B. Gautam, X. Liu, K. Zhang, F. Huang, J. H. Oh, H. Y. Woo, B. J. Kim, *Adv. Energy Mater.* **2018**, *8*, 1802674.
- [45] J. J. Samuel, A. Garudapalli, A. A. Mohapatra, C. Gangadharappa, S. Patil, N. P. B. Aetukuri, *Adv. Funct. Mater.* **2021**, *31*, 2102903.
- [46] T. L. Nguyen, C. Lee, H. Kim, Y. Kim, W. Lee, J. H. Oh, B. J. Kim, H. Y. Woo, *Macromolecules* **2017**, *50*, 4415.
- [47] S. Lee, Y. Kim, D. Kim, D. Jeong, G.-U. Kim, J. Kim, B. J. Kim, *Macromolecules* **2021**, *54*, 7102.
- [48] Y. Gao, J. Bai, Y. Sui, Y. Han, Y. Deng, H. Tian, Y. Geng, F. Wang, *Macromolecules* **2018**, *51*, 8752.
- [49] M. Moser, T. C. Hidalgo, J. Surgailis, J. Gladisch, S. Ghosh, R. Sheelamanthula, Q. Thiburce, A. Giovannitti, A. Salleo, N. Gasparini, A. Wadsworth, I. Zozoulenko, M. Berggren, E. Stavrinidou, S. Inal, I. Mcculloch, *Adv. Mater.* **2020**, *32*, 2002748.
- [50] S. Lee, Y. Kim, Z. Wu, C. Lee, S. J. Oh, N. T. Luan, J. Lee, D. Jeong, K. Zhang, F. Huang, T.-S. Kim, H. Y. Woo, B. J. Kim, *ACS Appl. Mater. Interfaces* **2019**, *11*, 45038.
- [51] S. Cong, J. Chen, B. Ding, L. Lan, Y. Wang, C. Chen, Z. Li, M. Heeney, W. Yue, *Mater. Horiz.* **2023**, *10*, 3090.
- [52] N.-K. Kim, S.-Y. Jang, G. Pace, M. Caironi, W.-T. Park, D. Khim, J. Kim, D.-Y. Kim, Y.-Y. Noh, *Chem. Mater.* **2015**, *27*, 8345.
- [53] M. McBride, N. Persson, D. Keane, G. Bacardi, E. Reichmanis, M. A. Grover, *ACS Appl. Mater. Interfaces* **2018**, *10*, 36464.
- [54] J. Y. Back, H. Yu, I. Song, I. Kang, H. Ahn, T. J. Shin, S.-K. Kwon, J. H. Oh, Y.-H. Kim, *Chem. Mater.* **2015**, *27*, 1732.

- [55] A. Giovannitti, R. B. Rashid, Q. Thiburce, B. D. Paulsen, C. Cendra, K. Thorley, D. Moia, J. T. Mefford, D. Hanifi, D. Weiyan, M. Moser, A. Salleo, J. Nelson, I. McCulloch, J. Rivnay, *Adv. Mater.* **2020**, *32*, 1908047.
- [56] M. Moser, A. Savva, K. Thorley, B. D. Paulsen, T. C. Hidalgo, D. Ohayon, H. Chen, A. Giovannitti, A. Marks, N. Gasparini, A. Wadsworth, J. Rivnay, S. Inal, I. McCulloch, *Angew. Chem., Int. Ed.* **2021**, *60*, 7777.
- [57] H. Jia, Z. Huang, P. Li, S. Zhang, Y. Wang, J.-Y. Wang, X. Gu, T. Lei, *J. Mater. Chem. C* **2021**, *9*, 4927.
- [58] Y. Wang, A. Hamidi-Sakr, J. Surgailis, Y. Zhou, H. Liao, J. Chen, G. Zhu, Z. Li, S. Inal, W. Yue, *J. Mater. Chem. C* **2021**, *9*, 13338.
- [59] K. Martin, J. Spickermann, H. J. Räder, K. Müllen, *Rapid Commun. Mass Spectrom.* **1996**, *10*, 1471.
- [60] C. R. Bridges, M. J. Ford, B. C. Popere, G. C. Bazan, R. A. Segalman, *Macromolecules* **2016**, *49*, 7220.
- [61] M. Li, H. Bin, X. Jiao, M. M. Wienk, H. Yan, R. A. J. Janssen, *Angew. Chem., Int. Ed.* **2020**, *59*, 846.
- [62] F. C. Spano, *Acc. Chem. Res.* **2010**, *43*, 429.
- [63] D. T. Duong, V. Ho, Z. Shang, S. Mollinger, S. C. B. Mannsfeld, J. Dacuna, M. F. Toney, R. Segalman, A. Salleo, *Adv. Funct. Mater.* **2014**, *24*, 4515.
- [64] S. G. Bucella, A. Luzio, E. Gann, L. Thomsen, C. R. McNeill, G. Pace, A. Perinet, Z. Chen, A. Facchetti, M. Caironi, *Nat. Commun.* **2015**, *6*, 8394.
- [65] S. Schott, E. Gann, L. Thomsen, S.-H. Jung, J.-K. Lee, C. R. McNeill, H. Sirringhaus, *Adv. Mater.* **2015**, *27*, 7356.
- [66] C. A. Thomas, K. Zong, K. A. Abboud, P. J. Steel, J. R. Reynolds, *J. Am. Chem. Soc.* **2004**, *126*, 16440.
- [67] T. Nguyen-Dang, S. Chae, J. Chatsirisupachai, H. Wakidi, V. Promarak, Y. Visell, T.-Q. Nguyen, *Adv. Mater.* **2022**, *34*, 2200274.
- [68] X. Wu, T. L. D. Tam, S. Chen, T. Salim, X. Zhao, Z. Zhou, M. Lin, J. Xu, Y.-L. Loo, W. L. Leong, *Adv. Mater.* **2022**, *34*, 2206118.
- [69] M. Ghittorelli, L. Lingstedt, P. Romele, N. I. Craciun, Z. M. Kovács-Vajna, P. W. M. Blom, F. Torricelli, *Nat. Commun.* **2018**, *9*, 1441.
- [70] M. Moser, L. R. Savagian, A. Savva, M. Matta, J. F. Ponder, T. C. Hidalgo, D. Ohayon, R. Hallani, M. Reisjalali, A. Troisi, A. Wadsworth, J. R. Reynolds, S. Inal, I. McCulloch, *Chem. Mater.* **2020**, *32*, 6618.
- [71] M. Moser, J. Gladisch, S. Ghosh, T. C. Hidalgo, J. F. Ponder, R. Sheelamantula, Q. Thiburce, N. Gasparini, A. Wadsworth, A. Salleo, S. Inal, M. Berggren, I. Zozoulenko, E. Stavrinidou, I. McCulloch, *Adv. Funct. Mater.* **2021**, *31*, 2100723.
- [72] D. Kim, H. Park, T. Kim, J.-W. Lee, D. Jeong, H.-I. Kwon, B. J. Kim, F. S. Kim, *Macromolecules* **2022**, *55*, 9039.
- [73] S. S. Hegedus, E. A. Fagen, *J. Appl. Phys.* **1992**, *71*, 5941.
- [74] J. Zhou, D. He, Y. Li, F. Huang, J. Zhang, C. Zhang, Y. Yuan, Y. Lin, C. Wang, F. Zhao, *Adv. Mater.* **2023**, *35*, 2207336.
- [75] H.-Y. Wu, C.-Y. Yang, Q. Li, N. B. Kolhe, X. Strakosas, M.-A. Stoeckel, Z. Wu, W. Jin, M. Savvakis, R. Kroon, D. Tu, H. Y. Woo, M. Berggren, S. A. Jenekhe, S. Fabiano, *Adv. Mater.* **2021**, *33*, 2106235.
- [76] D. Jeong, I.-Y. Jo, S. Lee, J. H. Kim, Y. Kim, D. Kim, J. R. Reynolds, M.-H. Yoon, B. J. Kim, *Adv. Funct. Mater.* **2022**, *32*, 2111950.
- [77] J. Xin, X. Meng, X. Xu, Q. Zhu, H. B. Naveed, W. Ma, *Matter* **2019**, *1*, 1316.
- [78] J.-W. Lee, D. Jeong, D. J. Kim, T. N.-L. Phan, J. S. Park, T.-S. Kim, B. J. Kim, *Energy Environ. Sci.* **2021**, *14*, 4067.
- [79] S. Sharma, A. K. Vats, L. Tang, F. Kaishan, J. Toyoda, S. Nagamatsu, Y. Ando, M. Tamagawa, H. Tanaka, M. Pandey, S. S. Pandey, *Chem. Eng. J.* **2023**, *469*, 143932.
- [80] S. Sharma, A. K. Vats, M. Pandey, S. Nagamatsu, J.-C. Chen, S. S. Pandey, *ACS Appl. Polym. Mater.* **2022**, *4*, 8315.
- [81] M. Pandey, Y. Sugita, J. Toyoda, S. Katao, R. Abe, Y. Cho, H. Bente, M. Nakamura, *Adv. Electron. Mater.* **2023**, *9*, 2201043.
- [82] S. Nagamatsu, W. Takashima, K. Kaneto, Y. Yoshida, N. Tanigaki, K. Yase, K. Omote, *Macromolecules* **2003**, *36*, 5252.
- [83] M. Pandey, H. Syafutra, N. Kumari, S. S. Pandey, R. Abe, H. Bente, M. Nakamura, *ACS Appl. Mater. Interfaces* **2021**, *13*, 38534.
- [84] L. Q. Flagg, C. G. Bischak, J. W. Onorato, R. B. Rashid, C. K. Luscombe, D. S. Ginger, *J. Am. Chem. Soc.* **2019**, *141*, 4345.